REVISTA MATÉRIA V.26 N.04
ISSN 1517-7076 articles e13097, 2021

Combined effects on Fe-Cr-C hardfacing deposited by new technique FCDW-GTAW

Fernando Henrique Gruber Colaço[1, 2],
Giuseppe Pintaude[2]

[1] Instituto Federal de Santa Catarina - IFSC, Department of Mechanics, Rua dos Imigrantes, 445, 89254-630, Santa Catarina, Jaraguá do Sul, Brazil.
[2] Universidade Tecnológica Federal do Paraná - UTFPR, Academic Department of Mechanics - PPGEM, Rua Deputado Heitor de Alencar Furtado, 5000, 81280-340, Paraná, Curitiba, Brazil.
e-mail: fernandogruber@ifsc.edu.br, pintaude@utfpr.edu.br

ABSTRACT

The hardfacing deposition with the GTAW process is widely studied with the addition of metallic powder or solid wire. This study introduces an original method, flux-cored-double-wire GTAW (FCDW-GTAW), where wires of different compositions are used simultaneously to deposit hardfacing. Because of the complexity in stabilizing the welding system, the combined effects of welding parameters should be investigated, allowing elaborate prediction models for the geometry and dilution of the deposits. These aspects are crucial for the target application, wear-resistant layers based on Fe-Cr-C composition, requiring a low-level of dilution and bead-geometry quality. Five parameters were chosen to model the deposition: the welding current, welding speed, standoff distance, torch angle, and wire feed pulse frequency. Therefore, using Response Surface Methodology with five factors at five levels to plan the experiments, thirty-two deposition conditions were necessary to model responses. Complete and reduced models were presented for width, reinforcement, penetration, and dilution responses. The reduced models showed a better prediction than the complete ones. The welding parameters' interaction was identified for the reduced models, where the welding current and speed were influential in all responses. Results showed the possibility of obtaining good quality in the beads applying the FCDW-GTAW technique.

Keywords: GTAW, double-wire, geometry, dilution, DOE-RSM.

1. INTRODUCTION

Wear-resistant coatings are widely used in the processing industry and are usually deposited by arc welding or thermal spray processes. Adequate processes for this application present low dilution and sound quality in the surface finish. Plasma transferred arc welding (PTAW), and gas tungsten arc welding (GTAW) are among the arc processes that provide these characteristics [1, 2]. Other processes, such as flux-cored arc welding (FCAW) and submerged arc welding (SAW), have a high deposition rate, but with a dilution above 30% where the effects of the substrate impair the abrasion resistance [3, 4]. Also, shielded metal arc welding (SMAW) is versatile in obtaining consumables but with a low deposition rate and low-quality coating surface finish.

The GTAW process using metallic power feed has been successful in increasing abrasion resistance [5]. However, the complexity of this deposit system is more significant than feeding the wire-shaped material.

When higher productivity and better aspect of the bead are required, a solution is to use the GTAW or PTAW process with wire fed from coils where the material supply is continuous, decreasing the process preparation time. In this line, solid cobalt-based wires are used for corrosion-resistant deposition coatings and have high quality and low dilution beads with both the GTAW and PTAW processes [6, 7].

Some strategies have been used to improve the bead quality during the GTAW process. CHEN *et al.* [8] adopted for this purpose a hot-wire feeding. In this case, they used a secondary welding source to heat the wire and control the deposition, transferring the metal through the current pulse. Another example regarding the GTAW process is linked with additive manufacturing. In this case, defects during deposition may be relevant. For this reason, GENG *et al.* [9] optimized the feeding system to correct the metal transfer failures related to the welding parameters and improve the accuracy during the deposition of the layer.

Autor Responsável: Fernando Henrique Gruber Colaço Data de envio: 21/10/2020 Data de aceite: 07/05/2021

10.1590/S1517-707620210004.1397

Another strategy would be the use of double-wire but is not so usual regarding the GTAW process. In other processes, double-wire can be used for improving the deposition rates. An improvement was achieved by WU *et al.* [10], who used double-arc with twin-wire of 316L steel through the GMAW process, obtaining higher deposition rates with the same welding energy, compared with the same deposits made with single-wire. In the same sense, ROSSINI *et al.* [11] evaluated that the double-wire tandem technique by the GMAW process also resulted in a reduction of the welding cycle. Finally, the investigation conducted by FENG *et al.* [12], whose deposition of the beads was carried out by double wire feeding through the plasma arc additive manufacturing process (DWF-PAM), increased in the deposition rate and better quality of the bead, considering the microstructure and mechanical properties.

Although some remarkable examples of double-wire can be found in the literature, for our knowledge, only the investigation performed by DEITOS FILHO *et al.* [13] to clad Inconel 625 alloy has used it associated with GTAW as a strategy to increase the deposition rate.The application of a similar technique for Fe-Cr-C based-alloy should probably consider the complexity of transformations from the feedstock material up to the end of solidification, as studied, for example, by CHAIDEMENOPOULOS *et al.* [14] during the FCAW process. Apart from this issue, a way to improve the welding quality predictions is through the RSM (Response Surface Methodology), which has been successfully used for the GTAW process.

SHANMUGAM and MURUGAN [1] deposited beads with GTAW to model the bead geometry and dilution using the central factorial composite experiment with three factors at five levels. They obtained models representing the results with a regression coefficient (R^2) above 94% for the geometry and 99% for the bead dilution.

KIAEE and AGHAIE-KHAFRI [15] applied the RSM to predict the tensile strength and hardness of A516-Gr70 carbon steel for connecting boiler parts by GTAW. The model presented by the authors indicates less than 5.45% variation that the model does not explain, that is, R^2 of 94.65%. Their models considered the shielding gas flow rate, current, and welding speed.

MADADI *et al.* [16] performed the optimization of the pulse parameters of the GTAW process for coatings with Stellite 6 using the RSM. They modeled the dilution and hardness of the layer with a prediction of the reduced model higher than that of the complete model, 85.2% (dilution), 82.2% (hardness) for complete models, and 86.7% and 85.5% for the reduced model, respectively. The results show that the reduced model forecasts better dilution and hardness of these coatings.

Finally, more recently, SARATHCHANDRA *et al.* [17] have applied the RSM methodology for the austenitic stainless-steel grade SS 304 deposited by wire arc additive manufacturing was made by using the Cold Metal Transfer (CMT) process. These authors studied the effect of welding current, welding speed, and standoff distance on four outputs: dilution, penetration, reinforcement, and width bead. They found optimum conditions for reducing the dilution level.

Given the lack identified in the literature cited above, there are no statistical studies on the beads' geometry using two tubular wires with different compositions for abrasion applications. This investigation aims to evaluate the influence of welding variables on the geometric characteristics of Fe-Cr-C hardfacing deposited by the process under development flux-cored-double-wire GTAW (FCDW-GTAW). This work presents as an innovation the simultaneous feed of two different fluxed wires to enable the selection of the microstructure obtained with the wires' combination. In this sense, the desired microstructure for abrasion applications can be determined using the combination of different wires associated with a low dilution deposition process. For this, an experimental design was carried out using the Response Surface Methodology (RSM) to gather and determine an adjustment between a complete model, using all the studied parameters and a reduced model. Besides, the welding parameters' effects were evaluated on the dilution and geometry of the weld bead. The microstructure obtained with the simultaneous welding of the two different wires was also detailed.

2. MATERIALS AND METHODS

Beads were deposited using an inverter power supply from the manufacturer Sumig model Lion 300 and a mechanized welding torch displacement system based on a stepper motor control system to control the welding speed. Two wires were added by a double feeding system built for this purpose consisting of two motors, support for the wire coils, and conduit coupled to the front of the welding torch.

Two wires with diameters of 1.6 mm were fed in a pulsed manner with pulse frequencies determined in the Design of Experiments (DoE). The wire feed speed is independent of the welding source and remained

fixed at 2 m/min when the feeders were activated as a function of the wire feed's pulse frequency. The wire feeders' angle was 160º concerning the weld bead plane, and the feed was directly into the fusion pool. The trials were performed pushing the weld pool.

The electrode used was tungsten doped with 1.5% Lanthanum. The tungsten electrode's diameter was 3.2 mm with the preparation angle and the tip length approximately 40º and 5 mm, respectively. The shielding gas used was Argon, with a flow rate of 14 l/min. The ceramic nozzle used was number 8, equipped with a gas lens, and the electrode was mounted outward at a distance of 5 mm. Even with the torch angle variation, the electrode tip was always kept in the same position regarding the wire feed system. For the realization of the beads, the double feeding configuration of flux-cored wires by the GTAW process was used, as shown in Figure 1 (a). The wires were positioned at an angle of 15º and directed to the tungsten electrode, and the contact tip was at a distance of 40 mm from the tungsten electrode, as shown in Figure 1 (c). The height of the wire feed was 2 mm, and the angle between the wires and the substrate was 20º, as shown in Figure 1 (d).

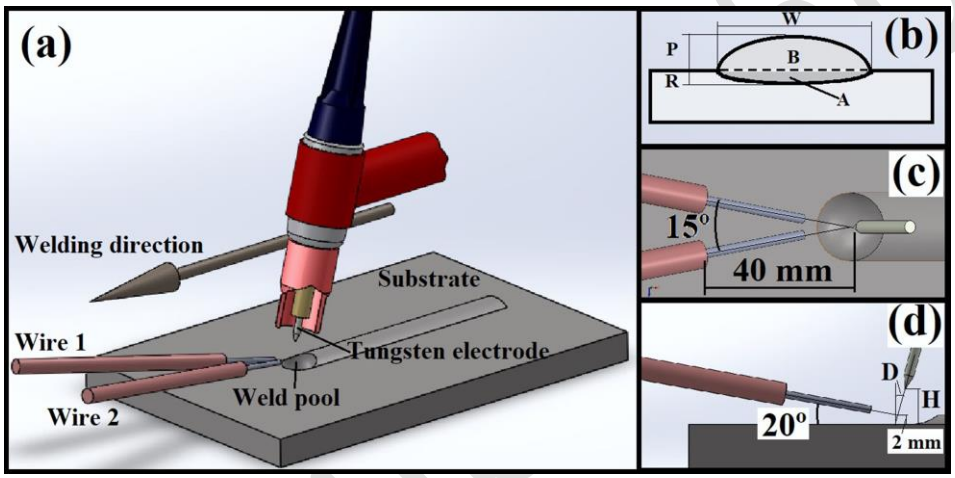

Figure 1: Welding scheme (a), (c), (d), and bead geometry and dilution parameters (b).

Data on current intervals, welding speed, and standoff distance used in the DoE were obtained through preliminary tests.

The parameters chosen for the deposition of the beads were the welding current (Im), welding speed (S), standoff distance (H), torch angle (D), and wire feed pulse frequency (F).

Two random wires with different chemical compositions but with characteristics of abrasion resistance of the deposit were deposited on a steel substrate with good weldability, forgeability, and toughness at low cost. AISI 1020 steel was used as a substrate, and the compositions of the two wires used for depositing the beads, named UTP 60 (DIN 8555 / MF-10-GF-60-GR) and UTP 68 (DIN 8555 / MF-10-GF-65-GR) are described in Table 1.

Workpieces with 200 x 150 x 6 mm³ dimensions were used to deposit three beads for each condition described in the section 'design of the experiments'. The samples' cross-section was used to obtain images of the bead geometry using the Image-Pro software. Geometry and dilution measurements were made in 6 beads for each process parameter condition. With these images, dilution (%D) was measured by the areas of penetration (A) and reinforcement (B) of the bead given in percentage, and the geometry was characterized by the width (W), the reinforcement (R), and penetration (P) of the bead, as shown in Figure1 (b) and Equation 1.

$$D = \left(\frac{Penetration\ area}{Total\ area}\right) * 100 = \left(\frac{A}{A+B}\right) \quad (1)$$

Table 1: Chemical composition of the substrate and wires.

	Chemical composition (Weight, %)											
	Carbon C	**Silicon Si**	**Manganese Mn**	**Chromium Cr**	**Molybdenum Mo**	**Tungsten W**	**Niobium Nb**	**Cobalt Co**	**Boron B**	**Sulfur S**	**Impurities II**	**Iron Fe**
AISI 1020 steel	0.18-0.23	-	0.3-0.6	-	-	-	-	-	-	Max 0.05	Max 0.04	Bal.
UTP 60	3.34	0.82	0.314	27.00	0.026	0.007	-	0.010	0.311	-	-	Bal.
UTP 68	3.41	1.05	0.228	17.88	-	-	3.06	-		-	-	Bal.

2.1. Design of the experiments

Some steps were carefully performed to achieve the objective of this study. These included selecting process parameters, planning and applying the experimental design, and measuring geometric parameters and bead dilution. Additional depositions were performed to confirm the reliability of the models.

With Minitab® software, the experimental design and development of the complete and reduced models for the width, reinforcement, and penetration of the bead were carried out, and the dilution.

In this study, a central composite design with five levels was used to determine the main characteristics and effects of the interaction between process parameters on the dilution and bead geometry, in addition to developing the complete and reduced empirical models for each response (W, R, P, and %D).

The process parameters with their respective value ranges are described in Table 2.

Table 2: Working range of process parameters.

Parameters			**Levels**				
		Notation	**-2**	**-1**	**0**	**1**	**2**
Welding current	A	Im	190	210	230	250	270
Welding speed	cm/min	S	5	10	15	20	25
Standoff distance	mm	H	8	10	12	14	16
Torch angle	º	D	5	10	15	20	25
Wire feed pulse frequency	Hz	F	30	45	60	75	90

Preheat temperature = 150 ºC, and six replicates for each condition described in Table 3.

The complete model considered the linear, quadratic terms and the interaction between the terms and can be expressed by the Y polynomial, according to Equation 2.

$$Y = +b_0 + b_1 I_m + b_2 S + b_3 H + b_4 D + b_5 F + b_{11} I_m^2 + b_{22} S^2 + b_{33} H^2 + b_{44} D^2 + b_{55} F^2 + b_{12} I_m * S + b_{13} I_m * H + b_{14} I_m * D + b_{15} I_m * F + b_{23} S * H + b_{24} S * D + b_{25} S * F + b_{34} H * D + b_{35} H * F + b_{45} D * F \quad (2)$$

The reduced model considered the terms statistically significant; that is, they were obtained from the complete model, excluding the terms that presented "p-value" greater than 0.05, which showed a confidence level below 95%. The adequacy coefficient R^2 and $R^2_{(adjusted)}$ was used to assess whether the model represents the test's data. $R^2_{(predicted)}$ values have used the parameters to determine the model's prediction quality for new observations. These data are represented in percentages and interpreted as the best prediction, the values closer to 100.

3. RESULTS AND DISCUSSION

The experimental design matrix with the process parameters' average values and the responses are described in Table 3.

Table 3: Development of the experiment and the geometry and dilution responses.

Nº	Encoded Values					Uncoded values					Responses			
	Im	S	H	D	F	Im	S	H	D	F	W	R	P	%D
1	-1	-1	-1	-1	1	210	10	10	10	75	9.65±1.02	3.62±0.36	0.60±0.07	8.80±1.10
2	1	-1	-1	-1	-1	250	10	10	10	45	14.65±0.75	2.61±0.24	1.53±0.37	26.93±2.91
3	-1	1	-1	-1	-1	210	20	10	10	45	7.02±2.45	2.77±0.52	0.35±0.22	10.65±6.86
4	1	1	-1	-1	1	250	20	10	10	75	8.88±0.41	2.31±0.14	0.80±0.11	19.74±3.63
5	-1	-1	1	-1	-1	210	10	14	10	45	12.25±2.04	3.42±0.17	0.93±0.19	15.36±3.40
6	1	-1	1	-1	1	250	10	14	10	75	17.25±1.12	2.37±0.25	0.81±0.23	23.28±2.35
7	-1	1	1	-1	1	210	20	14	10	75	7.69±20.1	2.57±1.17	0.19±0.12	3.51±2.51
8	1	1	1	-1	-1	250	20	14	10	45	9.52±0.41	2.25±0.67	0.75±0.07	16.53±4.46
9	-1	-1	-1	1	-1	210	10	10	20	45	10.30±1.39	3.69±1.30	1.00±0.12	16.36±3.73
10	1	-1	-1	1	1	250	10	10	20	75	14.46±0.70	2.56±0.23	1.10±0.55	26.17±5.96
11	-1	1	-1	1	1	210	20	10	20	75	7.05±0.28	2.76±0.10	0.57±0.16	12.33±3.87
12	1	1	-1	1	-1	250	20	10	20	45	8.96±0.52	2.31±0.28	0.92±0.19	25.01±3.98
13	-1	-1	1	1	1	210	10	14	20	75	10.29±1.27	3.70±0.44	0.54±0.16	9.35±2.01
14	1	-1	1	1	-1	250	10	14	20	45	16.26±0.73	2.72±0.15	1.30±0.50	23.79±5.94
15	-1	1	1	1	-1	210	20	14	20	45	6.15±0.61	3.04±0.27	0.26±0.07	4.18±1.40
16	1	1	1	1	1	250	20	14	20	75	9.34±0.54	2.24±0.22	0.56±0.13	14.90±2.71
17	-2	0	0	0	0	190	15	12	15	60	5.71±1.71	3.85±0.62	0.17±0.03	3.37±1.15
18	2	0	0	0	0	270	15	12	15	60	13.67±1.72	2.18±0.17	0.91±0.19	27.94±6.78
19	0	-2	0	0	0	230	5	12	15	60	19.20±3.47	3.19±0.35	1.53±0.29	31.90±6.12
20	0	2	0	0	0	230	25	12	15	60	7.30±0.65	2.17±0.48	0.72±0.09	8.41±4.07
21	0	0	-2	0	0	230	15	8	15	60	10.17±0.92	2.51±0.49	0.80±0.12	22.92±4.72
22	0	0	2	0	0	230	15	16	15	60	12.48±1.59	2.48±0.21	0.49±0.12	13.13±2.83
23	0	0	0	-2	0	230	15	12	5	60	8.61±0.53	2.96±0.28	0.65±0.15	15.60±2.53
24	0	0	0	2	0	230	15	12	25	60	8.44±1.13	3.22±0.26	0.72±0.12	14.99±1.40
25	0	0	0	0	-2	230	15	12	15	30	7.92±0.68	2.73±0.49	0.84±0.15	17.34±2.59
26	0	0	0	0	2	230	15	12	15	90	9.43±1.77	2.51±0.40	0.59±0.15	16.60±3.88
27	0	0	0	0	0	230	15	12	15	60	9.63±0.50	2.80±0.15	0.59±0.12	16.30±1.64
28	0	0	0	0	0	230	15	12	15	60	10.39±0.33	2.71±0.13	0.59±0.05	15.06±3.20
29	0	0	0	0	0	230	15	12	15	60	10.29±1.69	2.67±0.56	0.72±0.15	18.53±4.11
30	0	0	0	0	0	230	15	12	15	60	10.20±1.96	2.75±0.57	0.58±0.10	16.86±3.97
31	0	0	0	0	0	230	15	12	15	60	10.11±1.02	2.77±0.32	0.78±0.07	18.84±3.46
32	0	0	0	0	0	230	15	12	15	60	10.18±1.06	2.64±0.24	0.80±0.14	18.84±3.77

3.1. Development of the Empirical Model

The empirical model was developed for the width, penetration, reinforcement, and bead dilution deposited with GTAW in the configuration of two flux-cored wires.

Equations 3 to 10 show the complete and reduced models for width reinforcement, penetration, and bead dilution.

Complete and reduced models for the weld bead width response:

$$W_{Complete} = -14.5 + 0.178\ I_m + 0.375\ S - 2.02\ H + 0.552\ D + 0.035\ F - 0.000152\ I_m^2 + 0.03316\ S^2 + 0.0870\ H^2 - 0.01409\ D^2 - 0.001398\ F^2 - 0.00709\ I_m * S + 0.00478\ I_m * H + 0.00096\ I_m * D + 0.000329\ I_m * F - 0.0387\ S * H + 0.0022\ S * D + 0.0026\ S * F - 0.0328\ H * D + 0.00267\ H * F - 0.00047\ D * F \quad (3)$$

$$W_{Reduced} = -9.22 + 0.1997\ I_m + 0.037\ S - 2.141\ H + 0.03524\ S^2 + 0.1000\ H^2 - 0.00709\ I_m * S \quad (1)$$

Complete and reduced models for the weld bead reinforcement response:

$$R_{Complete} = 19.65 - 0{,}1182\ I_m - 0.3434\ S + 0.293\ H - 0{,}09\ D + 0.0315\ F + 0.000187 - 0{,}000355\ S^2 - 0.01378\ H^2 + 0.003745\ D^2 - 0.000106\ F^2 + 0.001375\ I_m * S - 0.00025\ I_m * H - 0.000288\ I_m * D - 0.000017\ I_m * F + 0.00175\ S * H - 0.00065\ S * - 0.0003\ S * F + 0.00713\ H * D - 0.00075\ H * F - 0.00317\ D * F \quad (2)$$

$$R_{Reduced} = +24.38 - 0.1337\ I_m - 0.3708\ S - 0.1069\ D - 0.00328\ F + 0.000203\ I_m^2 + 0.003996\ D^2 + 0.001375\ I_m * S \quad (3)$$

Complete and reduced models for the weld bead penetration response:

$$P_{Complete} = -7.04 + 0.0649\ I_m - 0.2419\ S + 0.220\ H + 0.0412\ D + 0.0014\ F - 0.000083\ I_m^2 + 0.004518\ S^2 - 0.00176\ H^2 + 0.000118\ D^2 + 0.000046\ F^2 - 0.000006\ I_m * S - 0.000516\ I_m * H - 0.000194\ I_m * D - 0.000123\ I_m * F - 0.00144\ S * H + 0.000375\ S * D + 0.001292\ S * F - 0.00206\ H * D - 0.000854\ H * F + 0.000375\ D * F \quad (4)$$

$$P_{Reduced} = -2.35 + 0.0488\ I_m - 0.2544\ S - 0.04479\ H - 0.02596\ F - 0.000084\ I_m^2 + 0.004500\ S^2 + 0.001292\ S * F \quad (5)$$

Complete and reduced models for the weld bead dilution response

$$D_{Complete} = -82.6 + 0.636\ I_m + 0.39\ S - 0.23\ H + 0.33\ D + 0.115\ F - 0.000924\ I_m^2 - 0.0197\ S^2 + 0.0557\ H^2 - 0.01839\ D^2 - 0.00018\ F^2 + 0.0013\ I_m * S + 0.0033\ I_m * H + 0.00325\ I_m * D - 0.00052\ I_m * F - 0.1026\ S * H + 0.026\ S * D + 0.00173\ S * F - 0.0834\ H * D - 0.0055\ H * F + 0.00153\ D * F \quad (6)$$

$$D_{Reduced} = -40.4 + 0.2877\ I\_m + 0.568\ S + 0.284\ H - 0.0427\ F - 0.1028\ S * H \quad (7)$$

Equations 4, 6, 8, and 10 presents only the terms with a significant probability of 95% for the reduced width, reinforcement, penetration, and bead dilution models.

3.2. Adequacy of the Developed Models

The dispersion diagrams were designed to highlight the degree of proximity between the predicted and observed values for the width, reinforcement, penetration, and dilution models, as shown in Figure 2.

It is possible to observe that the data indicate adequacy to the regression model. Another evidence that shows a high correlation between predicted values and observed values of the dilution and bead geometry is the adequacy coefficient (R^2) that indicates the conformity of the model's adjustment.

Figure 2 shows the adequacy coefficients R^2, $R^2_{(adjusted)}$, and $R^2_{(predicted)}$ for the complete and reduced width, reinforcement, penetration, and dilution models.

It is possible to perceive by the adequacy coefficient R^2 that the complete model adjusts well the data obtained in more than 97%, being compatible with the data found by SHANMUGAM and MURUGAN [1]. However, the $R^2_{(predicted)}$ prediction of this model for new depositions shows a low percentage of correct responses, except for reinforcement.

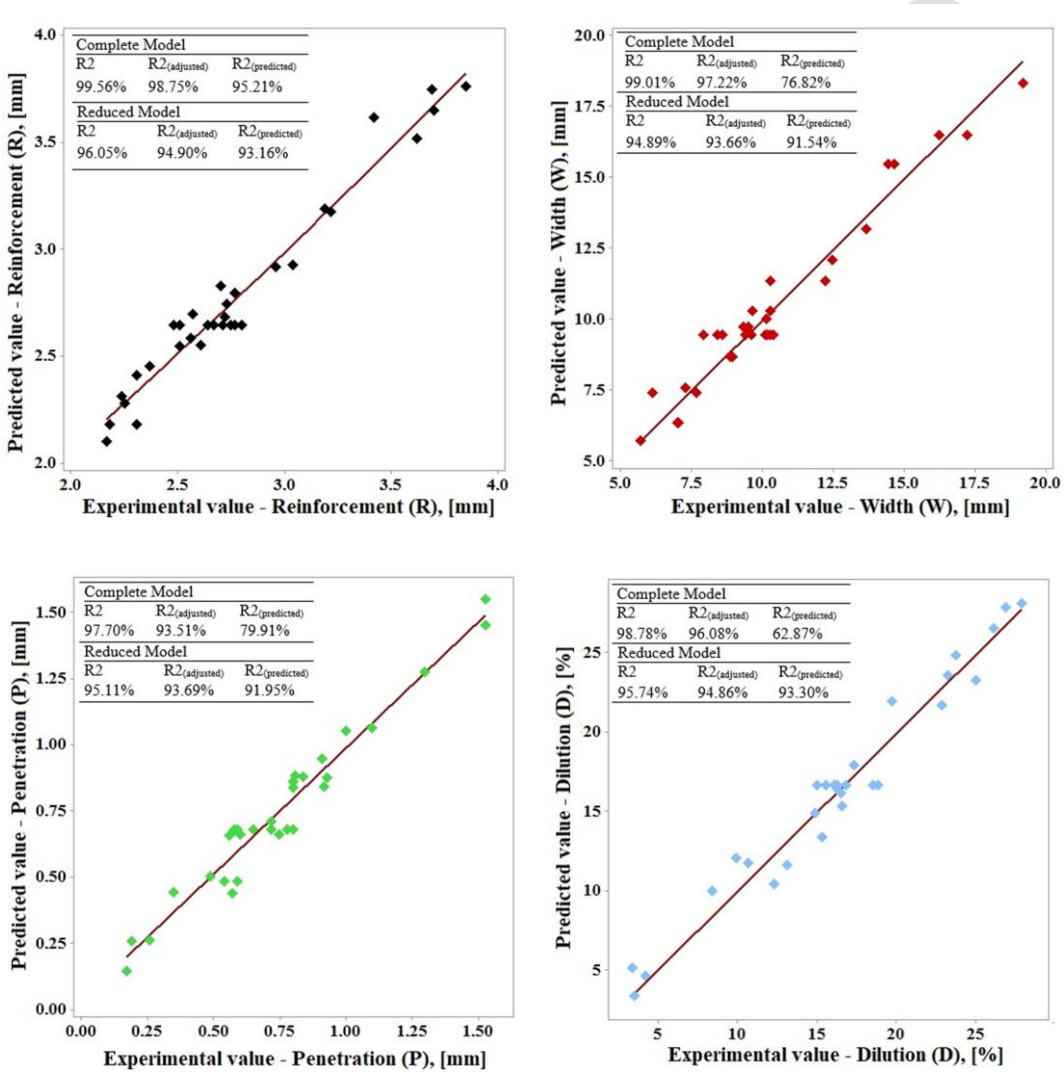

Figure 2: Comparison between the observed values and the predicted by the reduced width, reinforcement, penetration, and dilution models.

In the case of the reduced models, R^2 does not represent as well as the complete models. On the other hand, $R^2_{(predicted)}$ presents a considerable gain in predicting new analyzes for the reduced models with adequacy above 91% and higher than those found by THAO and KIM. [18] Also, the complete models are highly complex to replace the terms compared to the reduced model application, making it easier to use these models. Therefore, reduced models are preferred over complete models.

3.3. Direct Effect of Welding Parameters on the Bead

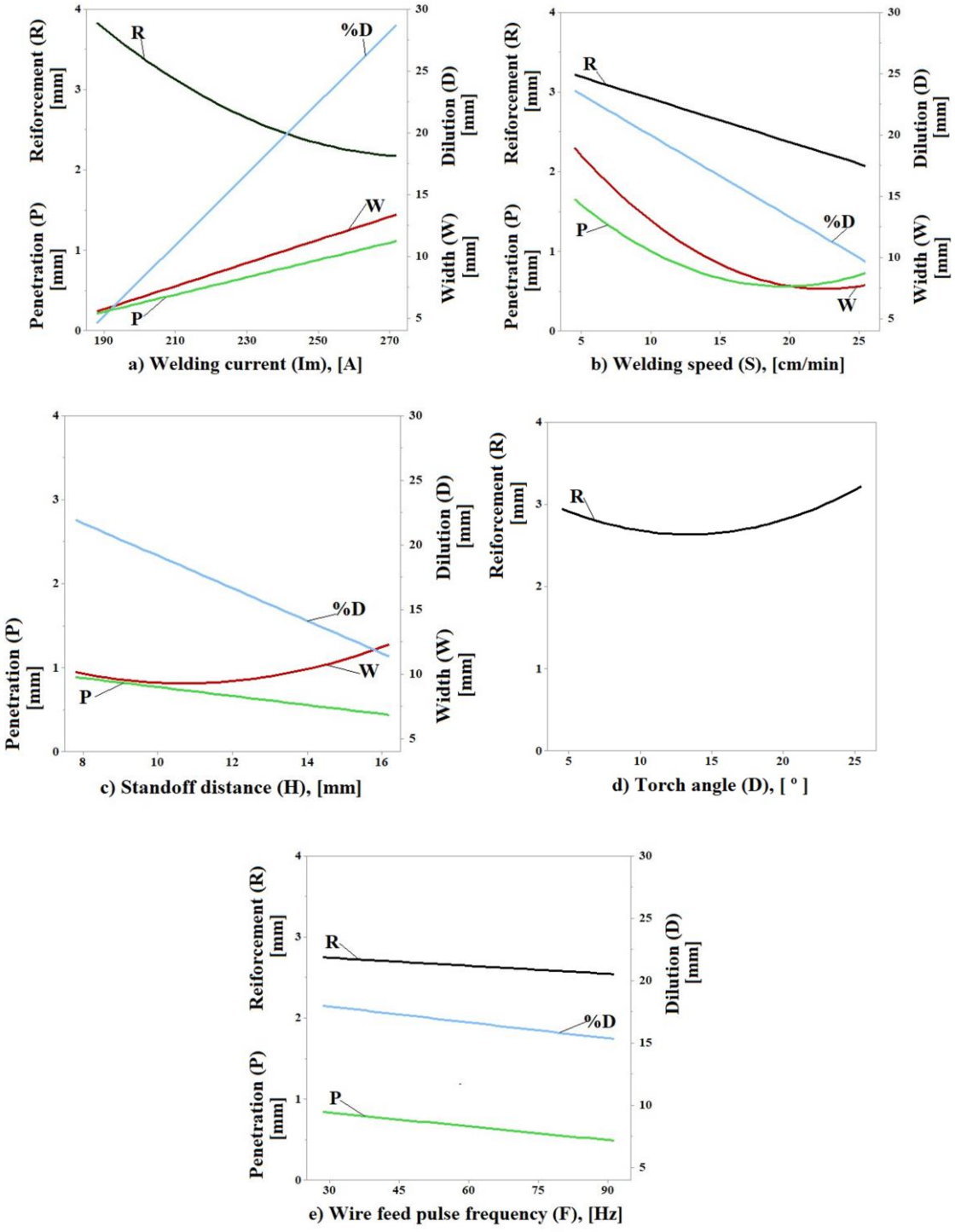

Figure 3: Effects of welding current (a), welding speed (b), standoff distance (c), torch angle (d), and wire feed pulse frequency (e) in width (W), reinforcement (R), penetration (P), and dilution (%D) of the weld bead.

As a consequence of the models obtained in these experiments, Figure 3 shows the effects of welding current (a), welding speed (b), standoff distance (c), torch angle (d), and wire feed pulse frequency (f) on the dilution and bead geometric parameters.

From Figure 3 (a), it is possible to verify that the welding current was responsible for reducing the reinforcement and increasing the width and penetration of the bead, providing an increase in dilution with the increase of the welding current. Similar behavior was found by BALASUBRAMANIAN *et al.* [19] and

SHANMUGAM and MURUGAN [1]. However, the intensity of the results of this work was higher mainly due to the volume of material deposited in the form of double wire. Also, the range of welding parameters was greater, showing better the effects of each welding parameter. In this sense, this behavior can be explained by the rise in temperature in the piece caused by the increase of the heat input to where the welding current increases [1, 20].

Another parameter that can influence the heat input is welding speed. In this case, the behavior of the bead width, dilution, and penetration was the opposite of that presented with the variation of the welding current, that is, the increase in the welding speed caused a reduction in the bead geometry, corroborating the behavior observed by GUPTA *et al.* [21]. The reinforcement maintained the reduction behavior due to the smaller amount of material added per unit of length with the increase in the welding speed.

On the other hand, the bead width reduction stabilizes, and the penetration increases again around 0.15 mm when the welding speed goes from 15 to 25 cm/min. This statement can be interpreted by analyzing Figure 3 (b). Besides, increasing the deposition speed results in a reduction in heat input and the volume of material deposited per unit length, even if the amount of wire fed does not change. However, SCOTTI and PONOMAREV [22] explain that the heat carried by the transferred drops that heat the base metal must be taken into account. One can use this assertion to explain the increase in penetration observed from the deposits applied with 20 cm/min, once the temperature transferred by the drops starts to have a small effect. Besides, another possible explanation for this trend could be associated with the uncertainties, resulting from the applied model itself.

The standoff distance effect occurs mainly in increasing the width and reducing penetration, resulting in a dilution reduction (Figure 3 c). According to TARNG and YANG [20] and BALASUBRAMANIAN *et al.* [23], the increase in the width of the bead is due to the increase in the area of projection or spreading of the arc voltaic caused by the increase in the standoff distance for electrodes with sharp points, in this case after 11 mm. Besides, increasing the standoff distance results in an increase in the voltaic arc voltage and the spread of the material surface's heat, reducing the penetration and, consequently, reducing the dilution. For minimal standoff distances, such as below 11 mm, the voltaic arc concentration increases and results in a greater capacity for melting the volume of material added, causing an increase in the bead's width and penetration. Occasionally, this behavior can also be interpreted as model uncertainty.

The angle of the torch affected less significantly only the reinforcement of the bead. From the 20º torch angle, the heat generated by the arc is spread, which causes an increase in the height of the bead reinforcement. For values less than 10º, the arc becomes more concentrated, and the bead narrower and bulkier.

The wire feed pulse frequency also presented results with low significance, as shown in Figure 3 (e), with only the reinforcement and penetration having a small reduction with the increase in the pulse frequency of the wire feed causing the dilution was also reduced, but these changes were not representative. The cycle time of the wire feed frequency is equal when the wires are not being added. Theoretically, the wire feed's pulse frequency should not affect the geometry of the bead, considering that the volume of material added does not change. However, the geometry was influenced due to the feeding system's inertia, reducing the feeding time, that is, for higher pulse frequencies of the wire feed, the smaller the volume of material added, resulting in a reduction in the bead geometry.

Figure 4 (a and b) shows the cross-section and the surface of a bead that presented good quality and geometry that was deposited with the parameters of condition 13 shown in Table 3. Obviously, in cases where the beads were deposited with low welding current, there was a lack of fusion of the wire, and the bead had an irregular appearance, as shown in Figure 4 (c and e), that was deposited with the parameters of condition 3 shown in Table 3. Also, in tests carried out to identify the effect of the wire direction, the beads showed the same lack of fusion behavior when the wires were directed to the arc's edge. That is when the distance between the wires was greater in the region of the voltaic arc. In these cases, the wires plunged into the weld pool and were partially fused, then the wires emerged to the surface of the part, forming bead with an irregular appearance. A scanline of detection by dispersive energy spectroscopy was carried out in the bead's cross-section to show the partial fusion of the wires and the result of the iron and chromium content shown in Figure 4 (d).

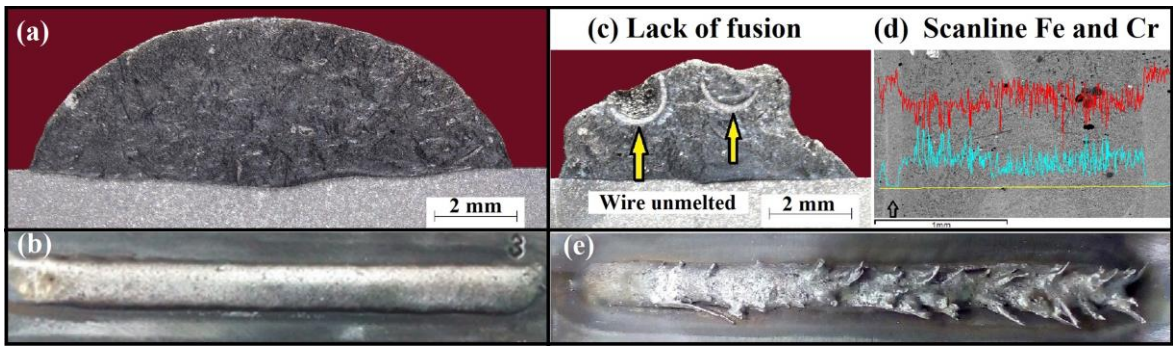

Figure 4: Cross-section and surface of a cord with good quality and geometry (a and b), cords with lack of fusion (c and e), and scanline showing the partially molten wire.

3.4. Effect of the Interaction of Welding Parameters on the Bead Quality

Figure 5 shows the effects of the interaction between the welding parameters present in the dilution, reinforcement, penetration, and bead width models.

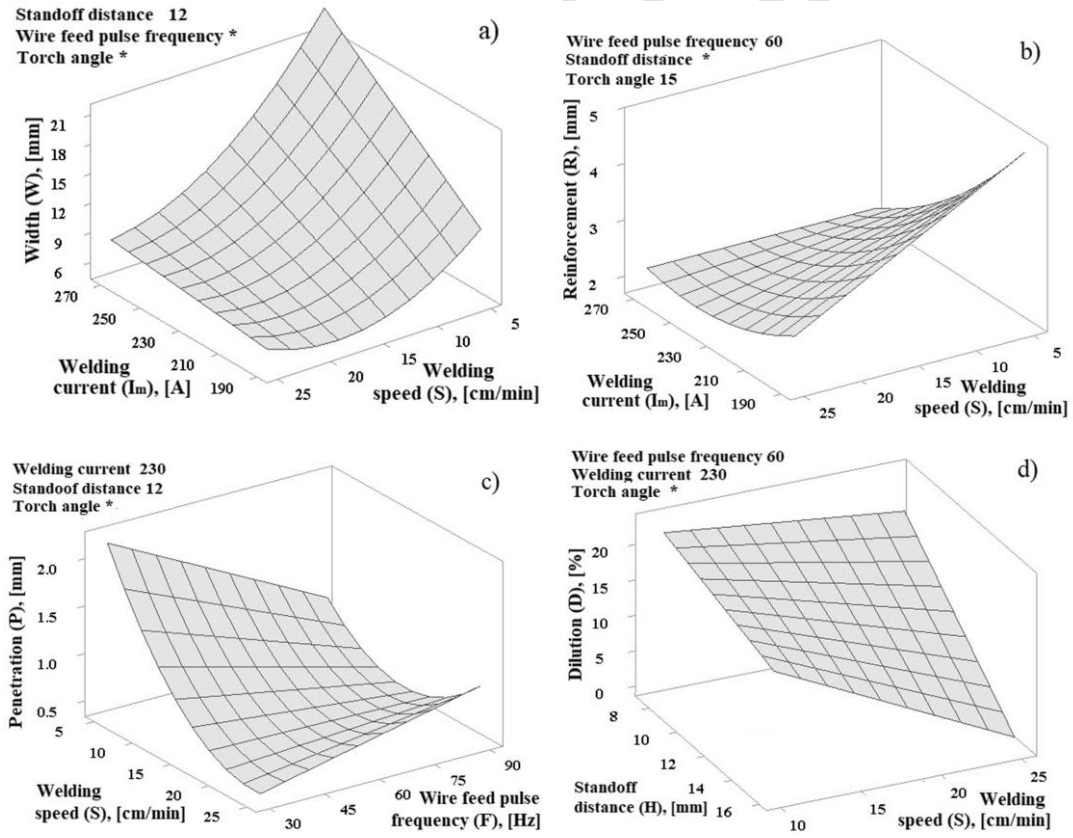

Figure 5: Effect of the interaction of the parameters on the width (W), reinforcement (R), penetration (P), and dilution (D) of the weld bead.

For the bead width, the process parameters significantly influential in the reduced model were the welding current and speed. They produced a more intense effect on high welding currents.The impact on the

bead width with the increase in the welding speed was more significant in 250 A than in 190 A, as shown in Figure 5 (a). This behavior can be explained by the increase in heat input, resulting from low speeds and high currents, contributing to the increase in the bead width. This behavior is corroborated by Shanmugam and Murugan's findings [1] with the interaction between current and welding speed. The reinforcement also had a significant interaction on the reduced model, the welding current, and speed. In this case, the effect on the reinforcement with the welding speed variation was more noticeable in low welding currents, as Shanmugam and Murugan found [1].

Figure 5 (b) shows a more critical reduction in reinforcement with the increase in welding speed in 190 A than in 250 A. The reduction of welding speed promotes an increase in the cumulated volume of deposit and the heat input. It implies an increase in reinforcement, mainly during low welding currents. Figure 5 (c) shows the interaction between the parameters welding speed and wire feed pulse frequency. It was significant in the bead penetration response, with a more noticeable reduction in penetration with an increase in welding speed in low wire feed pulse frequencies (30 Hz). With higher frequencies (75 Hz), the welding speed had less influence on the reduction of penetration. To explain this behavior, one should consider that the time in which the wire is not fed is larger in low frequencies. In this case, the heat input only melts the base-metal, contributing to high penetration, compared with high frequencies [23].

The interaction between the welding parameters was only significant for the dilution between the terms standoff distance and welding speed, with the perception of the welding speed variation only for greater distances between the electrode to the part. The same can be said for the standoff distance effect, which is more noticeable at high welding speeds, as shown in Figure 5 (d). The increase in standoff distance reduces the voltaic arc intensity, affecting the deposit's depth penetration and consequently reducing the dilution. This effect is pronounced with the reduction of the heat input generated by increasing the welding speed.

3.5. Reliability of Models

Additional experiments to verify the reliability of models were conducted under a current range of 185 to 250 A and welding speed placed within 10 and 25 cm/min. Fixed parameters for them were standoff distance of 10 mm, torch angle of 15º, and wire feed pulse frequency of 60 Hz. The resulted deposits are shown in Figure 6.

From these experiments, the values of width, reinforcement, penetration, and dilution were obtained by the same method of image analysis already described. The theoretical values were calculated from the models generated for each answer, and the relative error between the calculated and experimentally obtained values was calculated in this new set of trials. The relative errors for the complete models are 11.2% for width, 25.2% for reinforcement, 19.7% for penetration, and 3.1% for dilution. On the other hand, for the reduced model, the errors are 8.5% for width, 30.8% for reinforcement, 15.1% for penetration, and 5.7% for dilution. If one considers that the relative errors are close to the value of the determination coefficient ($R^2_{predict}$) for each answer, it can be concluded that both models, complete and reduced, are reliable.

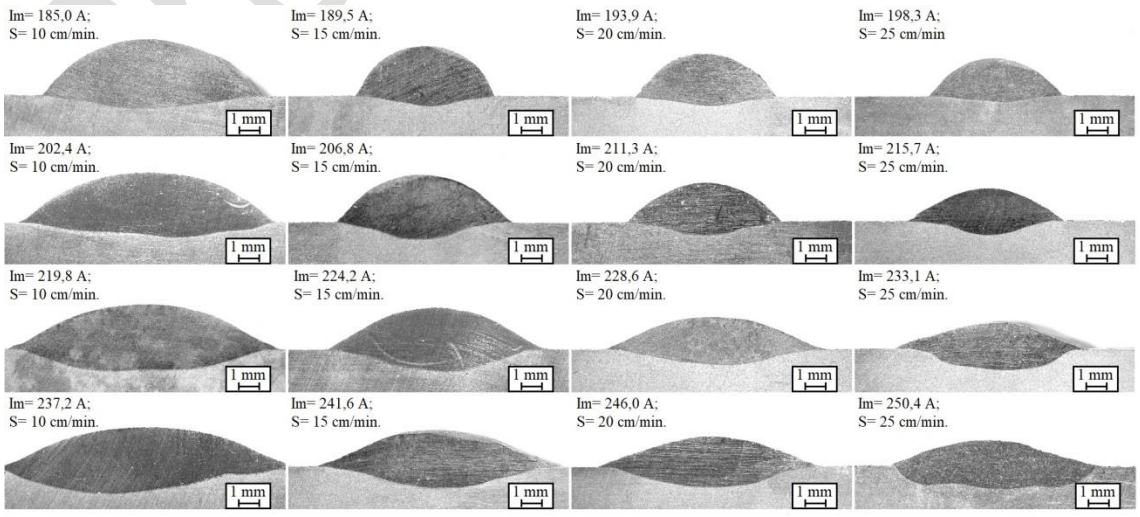

Figure 6: Cross-sectional images of deposits, showing the current and welding speed variations.

The additional experiments confirmed the main mechanism governing the bead geometry was the interaction between the welding current and speed, as shown in Figure 6. At low speeds, the heat input is enough to melt the volume of metal-wire. The exceeding heat acts reducing the reinforcement and increasing the penetration and width, being more pronounced for higher welding currents [23]. Therefore, an increase in heat input increases dilution, which can be detrimental to the microstructure in applications where abrasion resistance characteristics are required.

Besides, it was possible to observe that the beads showed good quality and adequate geometry for applications in coatings where abrasion resistance is required without harming the characteristics of the hardfacing. In this sense, the beads deposited with less thermal input showed good wettability and low penetration, and the beads deposited with greater heat input had greater dilution being undesired. This way, the use of Fe-Cr-C alloy tubular wires is preponderant to obtain coatings rich in carbides, as is the case of the wires used in this investigation. However, the deposit can be designed using wires with different compositions to obtain different microstructures and different properties. Figure 7 shows the microstructure obtained by the combined deposit of wires UTP 60 and UTP 68 using the parameters welding current of 230 A, welding speed of 15 cm/min, standoff distance of 10 mm, torch angle of 15º, and wire feed pulse frequency of 60 Hz. The microstructure is composed of primary chromium carbides, type M_7C_3, distributed by the eutectic matrix formed by austenite and chromium carbides. Similar microstructures were also obtained by LUZET *et al.* [24], and GENG *et al.* [25], and WANG *et al.* [26].

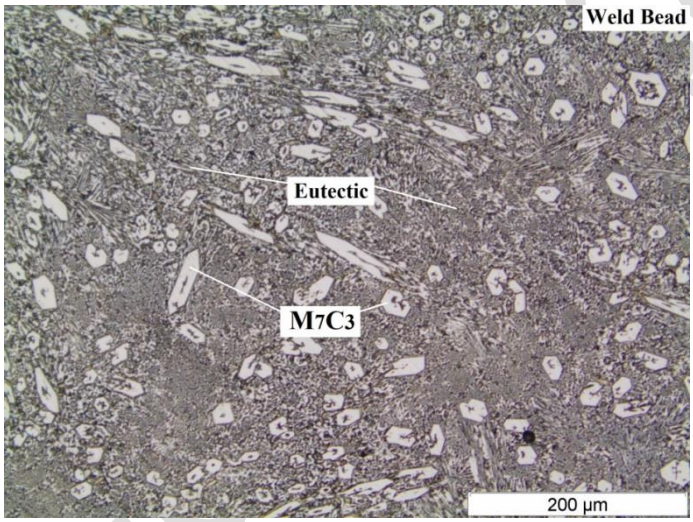

Figure 7: Deposit microstructure for hardfacing UTP 60 and UTP68.

4. CONCLUSIONS

A new technique to produce hardfacing beads, called FCDW-GTAW, was introduced. A series of experiments involving five input variables were investigated to produce hardfacing beads based on a wear-resistant composition. Four output parameters were modeled, giving rise to the following conclusions:

The width, reinforcement, and dilution reduced models predict more efficient analyses than complete models;

The welding current and speed are the most critical parameters that affect the bead geometry and dilution for the GTAW process during the FCDW-GTAW deposition of Fe-Cr-C hardfacing;

The welding speed was the most important parameter considering interactions in reduced models for all outputs of bead geometry;

The wire feed pulse frequency was only significant when interacting with the welding speed in the bead penetration response;

The standoff distance affected the arc voltage; consequently, it influenced the width and penetration of bead; and

It is possible to obtain good quality in the bead deposit with the FDCW-GTAW technique, opening the possibility to design diverse microstructures of wear-resistant layers.

5. ACKNOWLEDGMENTS

G. Pintaude acknowledges CNPq for the grant through Project no. 308416/2017-1. Authors thank IFSC through Application nº 05/2015/PROPPI. They also thank IMC – Engenharia de Soldagem through the donation of filters for the acquisition data.

6. BIBLIOGRAPHY

[1] SHANMUGAM, R., MURUGAN, N. "Effect of gas tungsten arc welding process variables on dilution and bead geometry of Stellite 6 hardfaced valve seat rings", DOI: 10.1179/174329406X126726. *Surface Engineering*, v. 22, n. 5, pp. 375-383, 2006.

[2] BALASUBRAMANIAN, V., VARAHAMOORTHY, R., RAMACHANDRAN, C.S., *et al.*, "Selection of welding process for hardfacing on carbon steels based on quantitative and qualitative factors", DOI: 10.1007/s00170-008-1406-8. *International Journal of Advanced Manufacturing Technology*, v. 40, pp. 887-897, 2009.

[3] COLAÇO, F.H.G., MARANHO, O. "Evaluation of mass loss of weld-deposited hardfacing with cored wire Ti-FeCrC alloy", DOI: 10.1080/09507116.2015.1096492. *Welding International*, v. 30, n. 4, pp. 283-292, 2016.

[4] SRIKARUN, B., OO, H.Z., PETCHSANG, S., *et al.*, "The effects of dilution and choice of added powder on hardfacing deposited by submerged arc welding", DOI: 10.1016/j.wear.2019.02.027. *Wear*, v. 424, pp. 246-254, 2019.

[5] WANG, X., SONG, S., ZOU, Z., *et al.*, "Fabricating TiC particles reinforced Fe-based composite coatings produced by GTAW multi-layers melting process", DOI: 10.1016/j.msea.2006.06.015. *Materials Science and Engineering: A*, v. 441, pp. 60-67, 2006.

[6] D'OLIVEIRA, A., PAREDES, R., SANTOS, R. "Pulsed current plasma transferred arc Hardfacing", DOI: 10.1016/j.jmatprotec.2005.02.269. *Journal of Materials Processing Technology*, v. 171, pp. 167-174, 2006.

[7] MIRSHEKARI, G.R., DAEE, S., BONABI, S.F., *et al.*, "Effect of interlayers on the microstructure and wear resistance of Stellite 6 coatings deposited on AISI 420 stainless steel by GTAW technique", DOI: 10.1016/j.surfin.2017.08.005. *Surfaces and Interfaces*, v. 9, pp. 79-92, 2017.

[8] CHEN, S., ZHANG, S., HUANG, N., *et al.*, "Droplet transfer in arcing-wire GTAW", DOI: 10.1016/j.jmapro.2016.05.014. *Journal of Manufacturing Processes*, v. 23, pp. 149-156, 2016.

[9] GENG, H., LI, J., XIONG, J., *et al.*, "Optimization of wire feed for GTAW based additive manufacturing", DOI: 10.1016/j.jmatprotec.2016.11.027. *Journal of Materials Processing Technology*, v. 243, pp. 40-47, 2017.

[10] WU, W., XUE, J., YAO, P. "A comparative study on single- and double-arc deposition processes", DOI: 10.1080/10426914.2020.1726947. *Materials and Manufacturing Processes*, v. 35, n. 3, pp. 346-353, 2020.

[11] FELIPE, L., ROSSINI, S., ANDRÉ, R., *et al.*, "Double-wire tandem GMAW welding process of HSLA50 steel", DOI: 10.1016/j.jmapro.2019.07.004. *Journal of Manufacturing Processes*, v. 45, pp. 227-233, 2019.

[12] FENG, Y., ZHAN, B., HE, J., *et al.*, "The double-wire feed and plasma arc additive manufacturing process for deposition in Cr-Ni stainless steel", DOI: 10.1016/j.jmatprotec.2018.04.040. *Journal of Materials Processing Technology*, v. 259, pp. 206-215, 2018.

[13] DEITOS FILHO, M.A., MARANHO, O., GANDELMAN, A., *et al.*, "Influence of the gas protection composition on dilution of 4130 80K material overlaid with 625 alloy by hot twin wire GTAW process", OTC Brasil 2015: The Atlantic: From East to West - An Ocean of Innovation, DOI: 10.4043/26194-ms. v. 1, pp .1227-1232, 2015.

[14] CHAIDEMENOPOULOS, N.G., PSYLLAKI, P., PAVLIDOU, E., *et al.*, "Aspects on carbides transformations of Fe-based hardfacing deposits", DOI: doi.org/10.1016/j.surfcoat.2018.10.061. *Surface & Coatings Technology*, v. 357, pp. 651-661, 2019.

[15] KIAEE, N. "Optimization of gas tungsten arc welding process by response surface methodology", DOI: 10.1016/j.matdes.2013.08.032. *Materials and Design*, v. 54, pp. 25-31, 2014.

[16] MADADI, F., ASHRAfiZADEH, F., SHAMANIAN, M. "Optimization of pulsed TIG cladding process of stellite alloy on carbon steel using RSM", DOI: doi.org/10.1016/j.jallcom.2011.08.073. *Journal of Alloys and Compounds*, v. 510, n. 1, pp. 71-77, 2012.

[17] SARATHCHANDRA, D.T., DAVIDSON, M.J., VISVANATHAN, G. "Parameters effect on SS304 beads deposited by wire arc additive manufacturing", DOI: 10.1080/10426914.2020.1743852. *Materials and Manufacturing Processes*, v. 35, n. 7, pp. 852-858, 2020.

[18] THAO, D.T., KIM, I.S. "Interaction model for predicting bead geometry for Lab Joint in GMA welding process", *Computational Materials Science and Surface Engineering*, v. 1, n. 4, pp. 237-244, 2009.

[19] BALASUBRAMANIAN, V., LAKSHMINARAYANAN, A.K., VARAHAMOORTHY, R., *et al.*, "Understanding the parameters controlling plasma transferred arc hardfacing using response surface methodology", *Materials and Manufacturing Processes*, DOI: 10.1080/15560350802316744. v. 23, n. 7, pp. 674-682, 2008.

[20] TARNG, Y.S., YANG, W.H. "Optimization of the weld bead geometry in gas tungsten arc welding by the taguchi method", DOI: 10.1007/BF01301698. *International Journal of Advanced Manufacturing Technology*, v. 14, n. 8, pp. 549-554, 1998.

[21] GUPTA, S.K., MEHROTRA, S., RAJA, A.R., *et al.*, "Effect of welding speed on weld bead geometry and percentage dilution in gas metal arc welding of SS409L", DOI: 10.1016/j.matpr.2019.07.497. *Materials Today: Proceedings*, v. 18, pp. 5032-5039, 2019.

[22] SCOTTI, A., PONOMAREV, V., Soldagem MIG/MAG, Melhor entendimento, Melhor desempenho. Brasil: Artliber Editora, 2008.

[23] BALASUBRAMANIAN, V., AK K. LAKSHMINARAYANAN, R. VARAHAMOORTHY, *et al.*, "Application of Response Surface Methodology to Prediction of Dilution in Plasma Transferred Arc Hardfacing of Stainless Steel on Carbon Steel." https://doi.org/10.1016/S1006-706X(09)60009-1. *Journal of Iron and Steel Research, International*, v. 16, no. 1, pp. 44–53, 2009.

[24] LUZ, H.A.S, TEIXEIRA, F.R., JUNIOR, M.A.B.P., *et al.*, "Aspectos Microestruturais e Do Comportamento Mecânico de Revestimento Duro Depositado Pelo Processo Arame Tubular", DOI: 10.1590/s1517-707620200002.1007. *Revista Matéria*, v. 25, n. 2, pp. 1-12, 2020.

[25] GENG, B., ZHOU, R., LI, L., *et al.*, "Change in Primary (Cr, Fe)7C3 Carbides Induced by Electric Current Pulse Modification of Hypereutectic High Chromium Cast Iron Melt", https://doi.org/10.3390/ma12010032. *Materials*, v. 12, n. 1, pp. 1-13, 2019.

[26] WANG, J., QI, X., XING, X., *et al.*, "Refinement of M_7C_3 in hypereutectic Fe-based hardfacing coating and interface behavior of (Ti, Nb)(C,N)/M_7C_3 from first-principles", https://doi.org/10.1088/2053-1591/ab27e3. *Materials Research Express*, v. 6, n. 8, pp. 1-12, 2019.

ORCID

Fernando Henrique Gruber Colaço https://orcid.org/0000-0001-5485-5635

Giuseppe Pintaude https://orcid.org/0000-0001-8215-4481